

# Holographic Description of the Phase Diagram of a Chiral Symmetry Breaking Gauge Theory

Nick Evans,<sup>\*</sup> Astrid Gebauer,<sup>†</sup> Keun-Young Kim,<sup>‡</sup> and Maria Magou<sup>§</sup>

*School of Physics and Astronomy,  
University of Southampton,  
Southampton, SO17 1BJ, UK*

The large  $N$   $\mathcal{N}=4$  gauge theory with quenched  $\mathcal{N}=2$  quark matter in the presence of a magnetic field displays chiral symmetry breaking. We study the temperature and chemical potential dependence of this theory using its gravity dual (based on the D3/D7 brane system). With massless quarks, at zero chemical potential, the theory displays a first order thermal transition where chiral symmetry is restored and simultaneously the mesons of the theory melt. At zero temperature, these transitions with chemical potential are second order and occur at different chemical potential values. Between the three there are two tri-critical points, the positions of which we identify. At finite quark mass the second order transition for chiral symmetry becomes a cross over and there is a critical point at the end of the first order transition, while the meson melting transition remains similar to the massless quark case. We track the movement of the critical points as the mass is raised relative to the magnetic field.

## I. INTRODUCTION

The phase diagram in the temperature chemical potential (or density) plane is a matter of great interest in both QCD and more widely in gauge theory [1–3]. In QCD there is believed to be a transition from a confining phase with chiral symmetry breaking at low temperature and density to a phase with deconfinement and no chiral symmetry breaking at high temperature. In the standard theoretical picture for QCD with massless quarks, the transition is first order for low temperature but growing density, whilst second order at low density and growing temperature. The second order transition becomes a cross over at finite quark mass. There is a (tri-)critical point where the first order transition mutates into the (second order) cross over transition. In fact though there could still be room in QCD for a more exotic phase diagram [3] as we will discuss in the context of our results in our final section.

In this paper we will present a precise holographic [4–6] determination of the phase diagram in the temperature chemical potential plane for a gauge theory that displays many of the features of the QCD diagram, although the precise details differ. A pictorial comparison of our theory to QCD can be made by comparing Fig 5 to Fig 10.

The theory we will consider is the large  $N$   $\mathcal{N}=4$  gauge theory with quenched  $\mathcal{N}=2$  quark matter [7–10] which has been widely studied [11]. An immediate difference between the  $\mathcal{N}=4$  glue theory and QCD is that the thermal phase transition to a deconfined phase occurs for infinitesimal temperature since the massless theory is con-

formal [5]. Essentially the entire temperature chemical potential phase diagram of our theory is therefore characterized by strongly coupled deconfined glue.

The quark physics is more subtle though - the phase diagram in the temperature chemical potential (density) plane for the  $\mathcal{N} = 2$  quark matter has been studied in [12–17]. When the quark mass is zero the theory is conformal and the origin of the phase diagram is a special point with confined matter. Immediately away from that point, in either temperature or chemical potential, a first order transition moves the theory to a deconfined theory (the mesons melt [18–20]).

When a quark mass is present in the  $\mathcal{N}=2$  theory the meson melting transition occurs away from the origin. This transition has been reported as first order with a second order transition point where the first order transition line touches the  $T = 0$  chemical potential axis [15, 16] (in the grand canonical ensemble). Interestingly there is a phase transition line in the temperature versus density plane (in the canonical ensemble) in which the quark condensate jumps [12, 13]. This area of the phase diagram is intrinsically unstable though and not realizable by imposing any chemical potential [16].

The crucial ingredient we will add to the theory is chiral symmetry breaking which will also bring the theory closer in spirit to QCD. As shown in [21–24] the  $\mathcal{N} = 2$  theory in the presence of a magnetic field displays chiral symmetry breaking through the generation of a quark anti-quark condensate. At zero density the finite temperature behaviour has been studied [21, 22] and there is a first order transition from a chiral symmetry broken phase at low temperature to a chiral symmetry restored phase at high temperature. In this paper we will include chemical potential as well to map out the full phase diagram in the temperature chemical potential plane. We will find a chiral symmetry restoration phase transition, which is first order for low density and second order for low temperature - there is a critical point where these

<sup>\*</sup>Electronic address: evans@soton.ac.uk

<sup>†</sup>Electronic address: ag806@soton.ac.uk

<sup>‡</sup>Electronic address: k.kim@soton.ac.uk

<sup>§</sup>Electronic address: mm21g08@soton.ac.uk

transitions meet. This physics is in addition to a meson melting transition which is first order at large temperature but apparently second order at low temperature. This latter region of transition is interesting because it is associated with a discontinuous jump from an embedding off the black hole to one that ends on it and it looks naively first order. However, when we plot any available order parameter in the boundary theory it appears second order.

We will also track the movement of these transition lines and critical points as the quark mass rises relative to the magnetic field. The infinite mass limit corresponds to the pure  $\mathcal{N}=2$  theory without magnetic field [14, 16]. The second order chiral symmetry restoration transition becomes a cross over the moment a mass is introduced. The first order transition structure though remains, even to the infinite mass limit, with two critical points: one is the end point of the first order transition and the other is the the end point of the second order meson melting transition. This structure was not reported in the results in [14, 16]<sup>1</sup> but this is not surprising since the structure, in that limit, is on a very fine scale. We have only found it by following the evolution of the larger structure present at low quark mass with a magnetic field. In addition we present evidence to suggest the parameter space with a second order meson melting transition extends away from just the  $T = 0$  axis, again, even in the infinite mass limit. We have confirmed these results in the strict  $B = 0$  limit also.

The theory we study may appear to be a rather vague relative of QCD with magnetic field induced chiral symmetry breaking. On the other hand it is a theory of strongly coupled glue with the magnetic field inducing conformal symmetry breaking in the same fashion as  $\Lambda_{\text{QCD}}$  in QCD. In fact the magnetic field case in the basic  $\mathcal{N}=4$  dual is the cleanest known example of chiral symmetry breaking in a holographic environment. Other deformations of the  $\mathcal{N}=4$  gauge theory typically lead to an ill-understood IR singular hard wall - see for example [25, 26]. The magnetic field case provides a smooth IR wall where we have more control but the results are likely to be the same in those more complex cases. We can hope to learn some lessons for a wider class of gauge theories.

## II. THE HOLOGRAPHIC DESCRIPTION

The  $\mathcal{N}=4$  gauge theory at finite temperature has a holographic description in terms of an  $\text{AdS}_5$  black hole

geometry (with  $N$  D3 branes at its core)[4-6]. The geometry is

$$ds^2 = \frac{r^2}{R^2}(-f dt^2 + d\vec{x}^2) + \frac{R^2}{r^2 f} dr^2 + R^2 d\Omega_5^2, \quad (1)$$

where  $R^4 = 4\pi g_s N \alpha'^2$  and

$$f := 1 - \frac{r_H^4}{r^4}, \quad r_H := \pi R^2 T. \quad (2)$$

Here  $r_H$  is the position of the black hole horizon which is related to the temperature  $T$ .

We will find it useful to make the coordinate transformation

$$\frac{dr^2}{r^2 f} \equiv \frac{dw^2}{w^2} \implies w := \sqrt{r^2 + \sqrt{r^4 - r_H^4}}, \quad (3)$$

with  $w_H = r_H$ . This change makes the presence of a flat 6-plane perpendicular to the horizon manifest. We will then write the coordinates in that plane as  $\rho$  and  $L$  according to

$$w = \sqrt{\rho^2 + L^2}, \quad \rho := w \sin \theta, \quad L := w \cos \theta, \quad (4)$$

The metric is then

$$ds^2 = \frac{w^2}{R^2}(-g_t dt^2 + g_x d\vec{x}^2) + \frac{R^2}{w^2}(d\rho^2 + \rho^2 d\Omega_3^2 + dL^2 + L^2 d\Omega_1^2), \quad (5)$$

where

$$g_t := \frac{(w^4 - w_H^4)^2}{2w^4(w^4 + w_H^4)}, \quad g_x := \frac{w^4 + w_H^4}{2w^4}. \quad (6)$$

### A. Quarks/D7 brane probes

Quenched ( $N_f \ll N$ )  $\mathcal{N}=2$  quark superfields can be included in the  $\mathcal{N}=4$  gauge theory through probe D7 branes in the geometry[7-10]. The D3-D7 strings are the quarks. D7-D7 strings holographically describe mesonic operators and their sources. The D7 probe can be described by its DBI action

$$S_{DBI} = -T_{D7} \int d^8 \xi \sqrt{-\det(P[G]_{ab} + 2\pi\alpha' F_{ab})}, \quad (7)$$

where  $P[G]_{ab}$  is the pullback of the metric and  $F_{ab}$  is the gauge field living on the D7 world volume. We will use  $F_{ab}$  to introduce a constant magnetic field (eg  $F_{12} = -F_{21} = B$ ) [21] and a chemical potential associated with baryon number  $A_t(\rho) \neq 0$  [13, 27].

We embed the D7 brane in the  $\rho$  and  $\Omega_3$  directions of the metric but to allow all possible embeddings must include a profile  $L(\rho)$  at constant  $\Omega_1$ . The full DBI action

<sup>1</sup> The existence of two critical points is related with the existence of the black hole to black hole transition. It is actually just visible in Fig 2c of [14] but the authors had not probed it in detail previously. After discussion of our results with the authors of [14], they have refined their computations and confirmed our results.

we will consider is then

$$S = \int d\xi^8 \mathcal{L}(\rho) = \left( \int_{S^3} \epsilon_3 \int dt d\vec{x} \right) \int d\rho \mathcal{L}(\rho), \quad (8)$$

where  $\epsilon_3$  is a volume element on the 3-sphere and

$$\begin{aligned} \mathcal{L} := & -N_f T_{D7} \frac{\rho^3}{4} \left( 1 - \frac{w_H^4}{w^4} \right) \\ & \times \sqrt{\left( 1 + (\partial_\rho L)^2 - \frac{2w^4(w^4 + w_H^4)}{(w^4 - w_H^4)^2} (2\pi\alpha' \partial_\rho A_t)^2 \right)} \\ & \times \sqrt{\left( \left( 1 + \frac{w_H^4}{w^4} \right)^2 + \frac{4R^4}{w^4} B^2 \right)}. \end{aligned} \quad (9)$$

Since the action is independent of  $A_t$ , there is a conserved quantity  $d$  ( $:= \frac{\delta S}{\delta F_{\rho t}}$ ) and we can use the Legendre transformed action

$$\tilde{S} = S - \int d\xi^8 F_{\rho t} \frac{\delta S}{\delta F_{\rho t}} = \left( \int_{S^3} \epsilon_3 \int dt d\vec{x} \right) \int d\rho \tilde{\mathcal{L}}(\rho), \quad (10)$$

where

$$\tilde{\mathcal{L}} := -N_f T_{D7} \frac{(w^4 - w_H^4)}{4w^4} \sqrt{K(1 + (\partial_\rho L)^2)} \quad (11)$$

$$\begin{aligned} K := & \left( \frac{w^4 + w_H^4}{w^4} \right)^2 \rho^6 + \frac{4R^4 B^2}{w^4} \rho^6 \\ & + \frac{8w^4}{(w^4 + w_H^4)} \frac{d^2}{(N_f T_{D7} 2\pi\alpha')^2}. \end{aligned} \quad (12)$$

To simplify the analysis we note that we can use the magnetic field value as the intrinsic scale of conformal symmetry breaking in the theory - that is we can rescale all quantities in (11) by  $B$  to give

$$\tilde{\mathcal{L}} = -N_f T_{D7} (R\sqrt{B})^4 \frac{\tilde{w}^4 - \tilde{w}_H^4}{\tilde{w}^4} \sqrt{\tilde{K}(1 + \tilde{L}'^2)}, \quad (13)$$

$$\tilde{K} = \left( \frac{\tilde{w}^4 + \tilde{w}_H^4}{\tilde{w}^4} \right)^2 \tilde{\rho}^6 + \frac{1}{\tilde{w}^4} \tilde{\rho}^6 + \frac{\tilde{w}^4}{(\tilde{w}^4 + \tilde{w}_H^4)} \tilde{d}^2, \quad (14)$$

where the dimensionless variables are defined as

$$\begin{aligned} & (\tilde{w}, \tilde{L}, \tilde{\rho}, \tilde{d}) \\ := & \left( \frac{w}{R\sqrt{2B}}, \frac{L}{R\sqrt{2B}}, \frac{\rho}{R\sqrt{2B}}, \frac{d}{(R\sqrt{B})^3 N_f T_{D7} 2\pi\alpha'} \right). \end{aligned} \quad (15)$$

In all cases the embeddings become flat at large  $\rho$  taking the form

$$\tilde{L}(\tilde{\rho}) \sim \tilde{m} + \frac{\tilde{c}}{\tilde{\rho}^2}, \quad \tilde{m} = \frac{2\pi\alpha' m_q}{R\sqrt{2B}}, \quad \tilde{c} = \langle \bar{q}q \rangle \frac{(2\pi\alpha')^3}{(R\sqrt{2B})^3}. \quad (16)$$

In the absence of temperature, magnetic field and density the regular embeddings are simply  $L(\tilde{\rho}) = \tilde{m}$ , which is the minimum length of a D3-D7 string, allowing us to identify it with the quark mass as shown.  $\tilde{c}$  should then be identified with the quark condensate with the relation shown.

We will classify the D7 brane embeddings by their small  $\tilde{\rho}$  behavior. If the D7 brane touches the black hole horizon, we call it a black hole embedding, otherwise, we call it a Minkowski embedding. We have used Mathematica to solve the equations of motion for the D7 embeddings resulting from (13). Typically in what follows, we numerically shoot out from the black hole horizon (for black hole embeddings) or the  $\tilde{\rho} = 0$  axis (for Minkowski embeddings) with Neumann boundary condition for a given  $\tilde{d}$ . Then by fitting the embedding function with (16) at large  $\tilde{\rho}$  we can read off  $\tilde{m}$  and  $\tilde{c}$ .

## B. Thermodynamic potentials

The Hamilton's equations from (10) are  $\partial_\rho d = \frac{\delta \tilde{S}}{\delta A_t}$  and  $\partial_\rho A_t = -\frac{\delta \tilde{S}}{\delta d}$ . The first simply means that  $d$  is the conserved quantity. The second reads as

$$\partial_\rho \tilde{A}_t = \tilde{d} \frac{\tilde{w}^4 - \tilde{w}_H^4}{\tilde{w}^4 + \tilde{w}_H^4} \sqrt{\frac{1 + (\tilde{L}')^2}{\tilde{K}}}, \quad (17)$$

where  $\tilde{A}_t := \frac{\sqrt{2} 2\pi\alpha' A_t}{R\sqrt{2B}}$ .

There is a trivial solution of (17) with  $\tilde{d} = 0$  and constant  $\tilde{A}_t$  [16]. The embeddings are then the same as those at zero chemical potential. For a finite  $\tilde{d}$ ,  $\tilde{A}_t$  is singular at  $\tilde{\rho} = 0$  and requires a source. In other words the electric displacement must end on a charge source. The source is the end point of strings stretching between the D7 brane and the black hole horizon. The string tension pulls the D7 branes to the horizon resulting in black hole embeddings [13]. For such an embedding the chemical potential ( $\tilde{\mu}$ ) is defined as [13, 27]

$$\begin{aligned} \tilde{\mu} := & \lim_{\tilde{\rho} \rightarrow \infty} \tilde{A}_t(\tilde{\rho}) \\ = & \int_{\tilde{\rho}_H}^{\infty} d\tilde{\rho} \tilde{d} \frac{\tilde{w}^4 - \tilde{w}_H^4}{\tilde{w}^4 + \tilde{w}_H^4} \sqrt{\frac{1 + (\tilde{L}')^2}{\tilde{K}}}, \end{aligned} \quad (18)$$

where we fixed  $\tilde{A}_t(\tilde{\rho}_H) = 0$  for a well defined  $A_t$  at the black hole horizon.

The Euclideanized on shell bulk action can be interpreted as the thermodynamic potential of the boundary field theory. The Grand potential ( $\tilde{\Omega}$ ) is associated with the action (9) while the Helmholtz free energy ( $\tilde{F}$ ) is as-

sociated with the Legendre transformed action (10):

$$\begin{aligned} \tilde{F}(\tilde{w}_H, \tilde{d}) &:= \frac{-\tilde{S}}{N_f T_{D7} (R\sqrt{B})^4 \text{Vol}} \\ &= \int_{\tilde{\rho}_H}^{\infty} d\tilde{\rho} \frac{\tilde{w}^4 - \tilde{w}_H^4}{\tilde{w}^4} \sqrt{\tilde{K}(1 + (\tilde{L}')^2)} \end{aligned} \quad (19)$$

$$\begin{aligned} \tilde{\Omega}(\tilde{w}_H, \tilde{\mu}) &:= \frac{-S}{N_f T_{D7} (R\sqrt{B})^4 \text{Vol}} \\ &= \int_{\tilde{\rho}_H}^{\infty} d\tilde{\rho} \frac{\tilde{w}^4 - \tilde{w}_H^4}{\tilde{w}^4} \sqrt{\frac{(1 + (\tilde{L}')^2)}{\tilde{K}}} \times \\ &\quad \left( \left( \frac{\tilde{w}^4 + \tilde{w}_H^4}{\tilde{w}^4} \right)^2 \tilde{\rho}^6 + \frac{1}{\tilde{w}^4} \tilde{\rho}^6 \right) \end{aligned} \quad (20)$$

where Vol denote the trivial 7-dimensional volume integral except  $\tilde{\rho}$  space, so the thermodynamic potentials defined above are densities, strictly speaking. Since  $\tilde{K} \sim \tilde{\rho}^6$ , both integrals diverge as  $\tilde{\rho}^3$  at infinity and need to be renormalized. Thermodynamic potentials, (18),(19) and (20) are reduced to  $B = 0$  case if we simplify omit all  $\frac{\tilde{\rho}^6}{\tilde{w}^4}$  and then tildes. See for example (21).

### III. CHIRAL SYMMETRY BREAKING AND THE THERMAL PHASE TRANSITION

We begin by reviewing the results of [21, 22] on magnetic field induced chiral symmetry breaking and the thermal phase transition to a phase in which the condensate vanishes. While they show the embeddings for fixed  $T$  and different values of  $B$ , we will show the embeddings for fixed  $B$  and different values of  $T$ . By fixing  $B$  we are using it as the intrinsic scale of symmetry breaking in the same fashion as  $\Lambda_{QCD}$  plays that role in QCD.

Let us digress here to explain how to understand the figures we will present in this paper. For example, in Fig 1 we have three columns. The left is the D7 brane embedding configuration. The middle shows a plot of the allowed values of the condensate  $\tilde{c}$  as a function of the quark mass  $\tilde{m}$  - these are thermodynamical conjugate variables. The right is the corresponding thermodynamic potential. Each row is for a fixed parameter we are varying - here it's temperature. The left and middle plots are plotted by solving the equation of motion (13) with the black hole boundary condition that the embedding is orthogonal to the horizon.

The right hand plot is calculated using (19) or (20). Both are the same at zero density. We subtract  $\lim_{\tilde{\rho} \rightarrow \infty} \frac{1}{4} \tilde{\rho}^4$  to remove the common infinite component.

Every *point* in the middle and right plots corresponds to one embedding *curve* in the left plot. These points are color coded with the colors common across each of the three plots. The order of colors follows the rainbow from the bottom embedding as a mnemonic.

In the middle plot we can find any transition point by a Maxwell construction (an equal area law), which is also confirmed by the minimum of the grand potential on the right. The vertical dashed line in the middle and right hand plots corresponds to the transition point.

In the left plots the gray region contains embeddings that are excluded since they are unstable, as shown in the middle and on the right.

The results for the case of a constant magnetic field and varying temperature are displayed in Fig 1a-d. The Fig 1a (Left) shows the D7 embeddings when  $T \ll B$  and the black hole is small. The embeddings are driven away from the origin of the  $\tilde{L} - \tilde{\rho}$  plane - this behaviour is a result of the inverse powers of  $\tilde{w}$ , when  $\tilde{w}_H \ll 1$ , in the Lagrangian (13) which lead the action to grow if the D7 approaches the origin (note that the factor of  $\tilde{\rho}^3$  multiplying the action means the action will never actually diverge). There is also a embedding that end on the black hole (shown in red) but they are thermodynamically disfavoured as shown in Fig 1a (Right).

At large  $\tilde{\rho}$  the stable embedding with  $\tilde{m} = 0$  has a non-zero derivative so  $\tilde{c}$  is non-zero and there is a chiral condensate *i.e.* chiral symmetry breaking. The U(1) symmetry in the  $\Omega_1$  direction is clearly broken by any particular embedding too. We can numerically read off the values of  $\tilde{m}$  and  $\tilde{c}$  from the embeddings and their values are shown in Fig 1a (Middle), where the dotted blue curves are for Minkowski embeddings, whilst the red curves are for black hole embeddings.

If the temperature is allowed to rise sufficiently then the black hole horizon grows to mask the area of the plane in which the inverse  $\tilde{w}$  terms in the Lagrangian are large. At a critical value of  $T$  the benefit to the  $\tilde{m} = 0$  embedding of curving off the axis becomes disfavoured and it instead lies along the  $\tilde{\rho}$  axis - chiral symmetry breaking switches off. This first order transition occurs at  $\tilde{w}_H = 0.2516$  as shown in Fig 1b by Maxwell's construction (Middle) and by lower grand potential (Right). Our value for the critical temperature agrees with the value  $\tilde{B} = 16$  in [22] since our  $\tilde{w}$  is the same as  $\sqrt{\frac{1}{B}}$  in [22].

We show an example of the embeddings above the critical temperature, their grand potential and the evolution of the curves in the  $\tilde{m} - \tilde{c}$  plane in Fig 1c.

The Fig 1d shows a case when  $T \gg B$  when the area of the plane in which B is important is totally masked by the black hole and the results match those of the usual finite T version of the  $\mathcal{N}=2$  theory. For  $\tilde{m} > \tilde{u}_H$  the embeddings are Minkowski like whilst for small  $\tilde{m}$  they fall into the black hole. There is a first order phase transition between these two phases which is the meson melting phase transition discussed in detail in [28–32]. Minkowski embeddings have a stable mesonic spectrum [10] whilst in the case of black hole embeddings the black holes' quasinormal modes induce an imaginary component to the meson masses [18, 19]. We can see that the previously reported “meson melting” transition at large quark mass

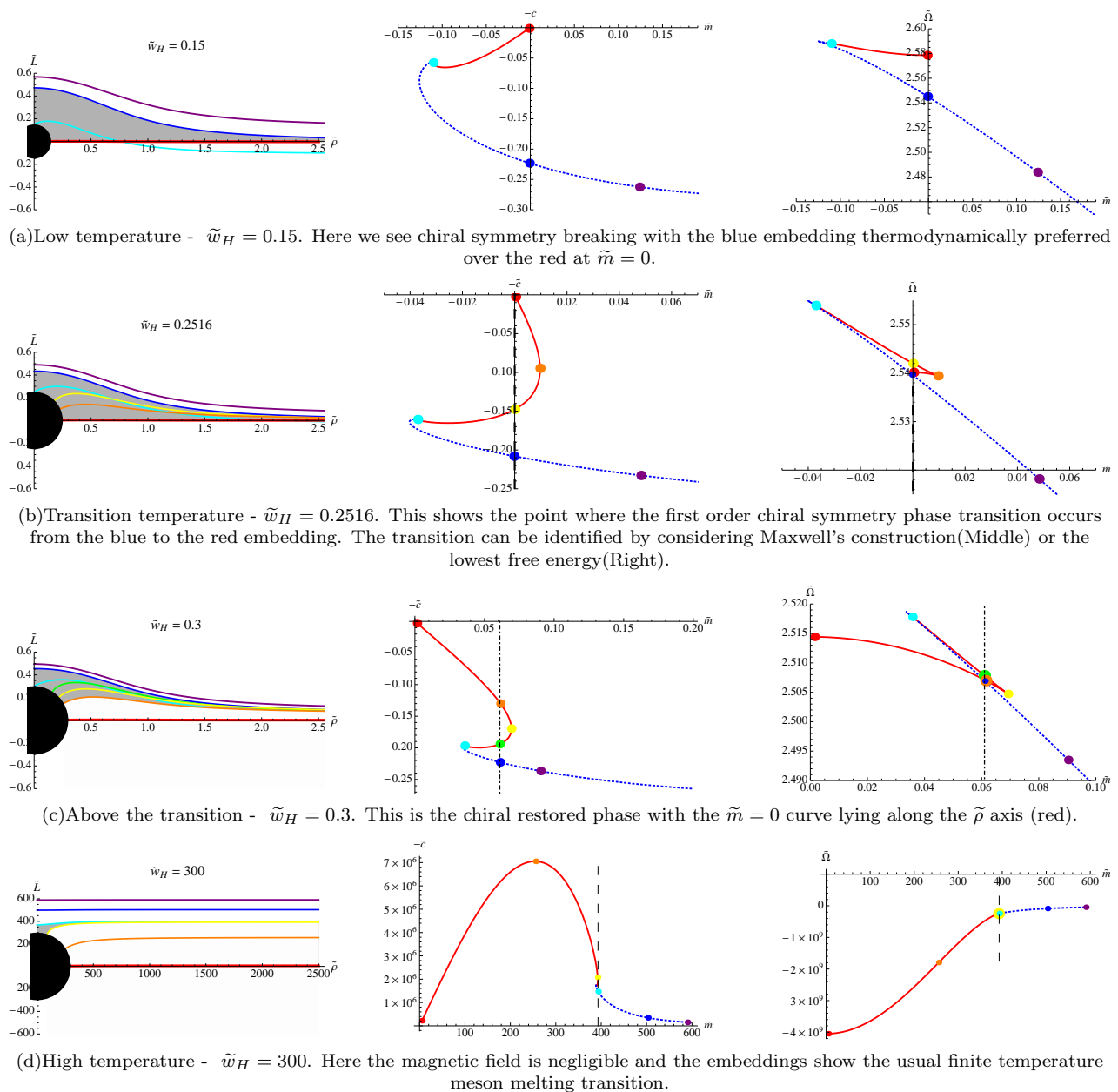


FIG. 1: The D7 brane embeddings(Left), their corresponding  $\tilde{m} - \tilde{c}$  diagrams(Middle), and the Free energies(Right) in the presence of a magnetic field at finite temperature. (Parameters are scaled or  $B = 1/2R^2$  in terms of parameters without tilde.)

becomes also the chiral symmetry restoring transition at zero quark mass.

#### IV. FINITE DENSITY OR CHEMICAL POTENTIAL AT ZERO TEMPERATURE

We can now turn to the inclusion of finite density or chemical potential in the theory with magnetic field. In this section we consider the zero temperature ( $\tilde{u}_H = 0$ ) theory only, and will continue to finite temperature in the next section.

A finite density (chemical potential) at zero temperature has been studied in the  $\mathcal{N}=2$  theory without a magnetic field in [15], where analytic solutions for both a black hole like embedding and a Minkowski embedding have been found. When a magnetic field is turned on, analytic solutions are not available any more, but we have found numerical solutions that continuously deform from the known analytic solutions at zero magnetic field.

Minkowski embedding solutions correspond to zero density and finite chemical potential. The black hole like embedding is the embedding deformed by the density - a spike forms from the D7 down to the origin of the  $\tilde{L} - \tilde{\rho}$

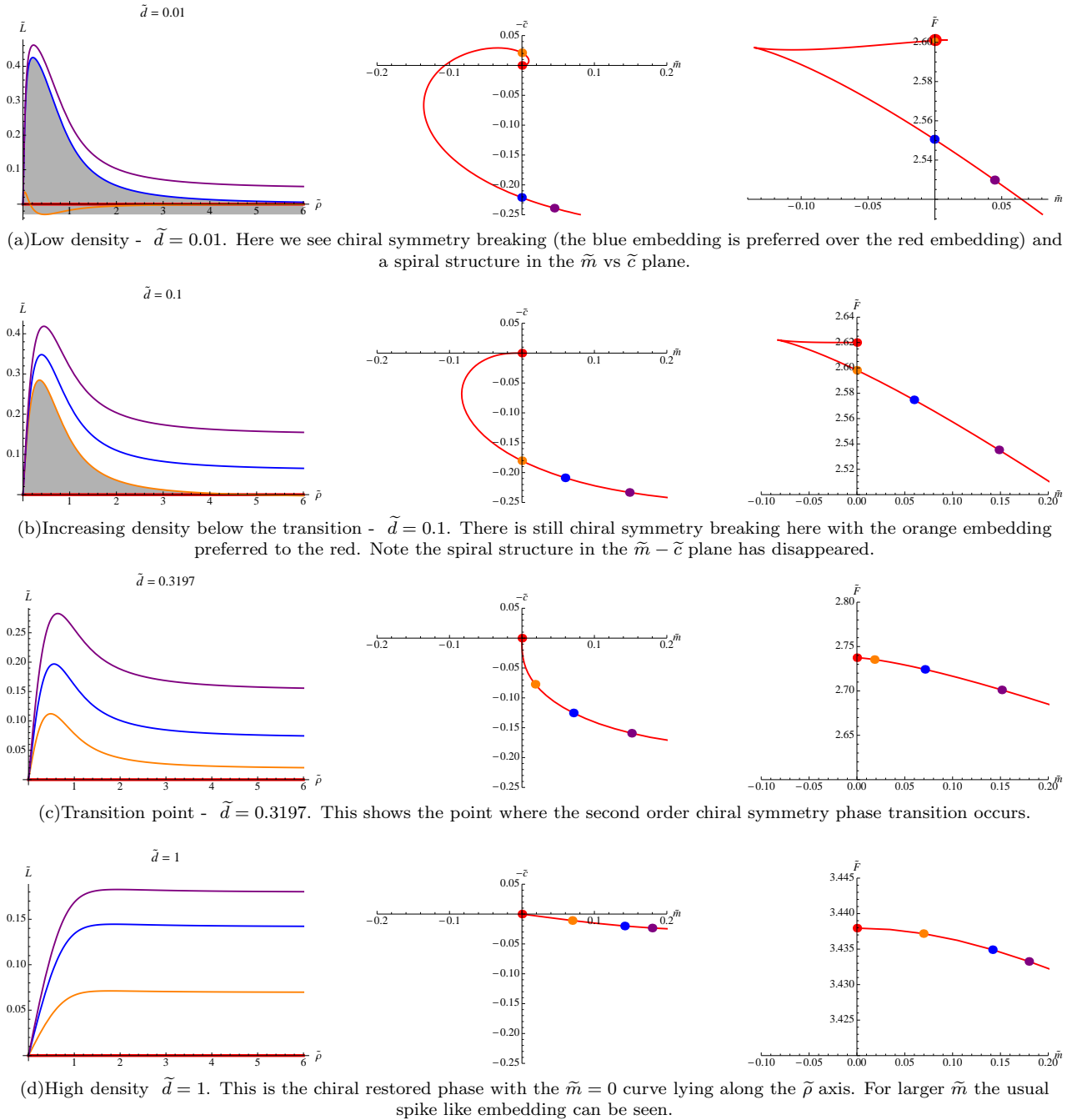


FIG. 2: The D7 brane embeddings(Left), their corresponding  $\tilde{m} - \tilde{c}$  diagrams(Middle), and the Free energies(Right) in the presence of a magnetic field at finite density. (Parameters are scaled or  $B = 1/2R^2$  in terms of parameters without tilde.)

plane (Fig 2d (Left)) which has been interpreted as an even distribution of strings (*i.e.* quarks) forming in the vacuum of the gauge theory.

First of all it will be interesting to see how the repulsion from the origin induced by a magnetic field and the attraction to the origin by the density compete. Thus we start with the canonical ensemble (that is solutions with non-zero  $\tilde{d}$ ) and consider black hole like embeddings exclusively. The plot in Fig 2a (Left) shows the embed-

dings for a small value of density. The solutions show the chiral symmetry breaking behaviour induced by the magnetic field but then spike to the origin by the density at small  $\tilde{\rho}$ . For  $\tilde{m} = 0$  one should compare the blue and red embeddings - the blue one is thermodynamically preferred as shown in Fig 2a (Right) The theory shows similar behavior to that seen at zero density: there is a spiral structure in the  $\tilde{m}$  vs  $\tilde{c}$  plane (Fig 2a (Middle)) [21]. That will disappear as the density increases.

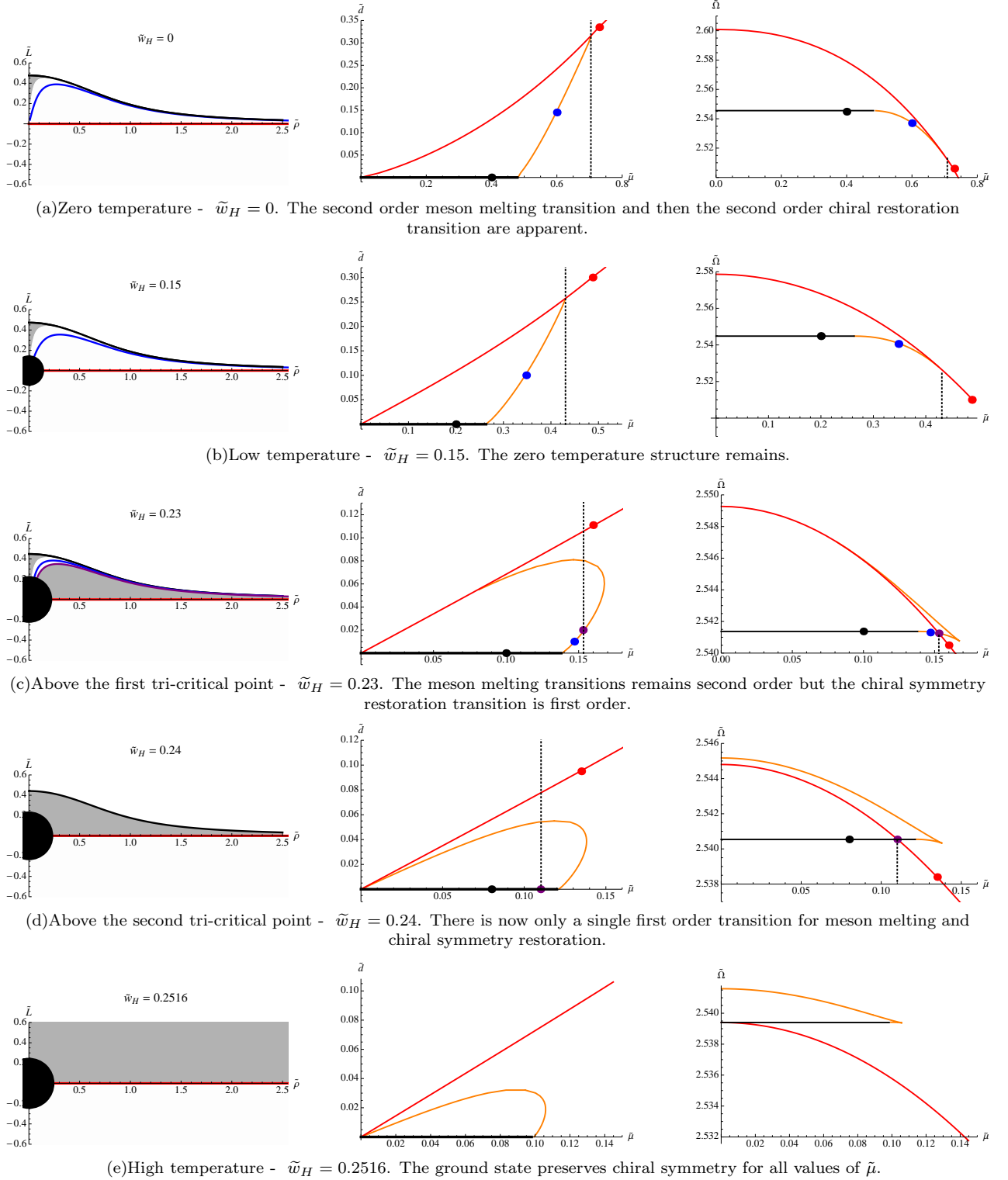


FIG. 3: The D7 brane embeddings (Left), their corresponding  $\tilde{d} - \tilde{\mu}$  diagrams (Middle), and the grand potentials (Right) for massless quarks in the presence of a magnetic field at a variety of temperatures that represent slices through the phase diagram Fig 5. (Parameters are scaled or  $B = 1/2R^2$  in terms of parameters without tilde.)

As the density increases the value of the condensate for the  $\tilde{m} = 0$  embeddings falls - we show a sequence of plots for growing  $\tilde{d}$  in Fig 2b-d (Middle). There is a critical value of  $\tilde{d} = 0.3197$  where  $\tilde{c}$  becomes zero for the massless embeddings - above this value of  $\tilde{d}$ , D7 embedding is flat and lies along the  $\tilde{\rho}$  axis (2c-d (Left)). One can see from the plots that there is a second order phase transition to a phase with no chiral condensate. In Fig 2c (Left) and 2d (Left) we show embeddings at the critical value of  $\tilde{d}$  and above it respectively. At very large density the solutions become the usual spike embeddings of the  $\mathcal{N} = 2$  theory at zero magnetic field.

We are not yet done though since there are also Minkowski embedding with zero density but constant chemical potential. These can have lower energy and be the preferred vacuum at a given value of chemical potential - that is, they are important in the Grand Canonical Ensemble. The relevant analysis is in Fig 3a (Fig 3b-e will be explained in the next section). On the left it shows the three possible types of embedding of the D7 for a given chemical potential at zero temperature. The black curve is the Minkowski embedding (with  $\tilde{d} = 0$ ), the blue the chiral symmetry breaking spike embedding (with  $\tilde{d} \neq 0$ ) and the red the chiral symmetry preserving black hole embedding (with  $\tilde{d} \neq 0$ ). Strictly speaking there is a fourth embedding which lies along the  $\tilde{\rho}$  axis and has constant  $A_t = \mu$  - its energy is equal for all  $\tilde{\mu}$  to that of the red embedding at  $\tilde{\mu} = 0$  and is never preferred over the red embedding with density, so we will ignore it hence forth. The trajectory of the three key embeddings in the  $\tilde{d} - \tilde{\mu}$  space is shown in the middle plot (note that again these two variables are thermodynamical conjugate variables). Finally on the right the grand potential is computed. Clearly at low chemical potential the Minkowski embedding is preferred and  $\tilde{d} = 0$ . There is a critical value of  $\tilde{\mu} = 0.470$  at which a transition occurs to the spike embedding. This transition looks naively first order since it is a transition between a Minkowski embedding and a black hole embedding. However, we can see that the Grand Potential appears smooth and the quark density is continuous, which is shown again in Fig.4a. The solid lines in Fig 4a are calculated from (18), which is based on the holographic dictionary. The dotted lines are obtained by numerically differentiating the grand potential ( $\tilde{d} = -\frac{\partial\tilde{\Omega}}{\partial\tilde{\mu}}$ ), which comes from a thermodynamic relation. This is a nontrivial consistency check of the holographic thermodynamics as well as our calculation [27, 33].

Further in Fig 4b we plot the behaviour of the quark condensate through this transition. The density and quark condensate are both smooth and the transition looks clearly second order. Here we have tested the smoothness numerically at better than the 1% level. Whether there is some other order parameter that displays a discontinuity is unclear but it would be surprising that any order parameter were smooth, were the transition first order. We conclude the transition is second

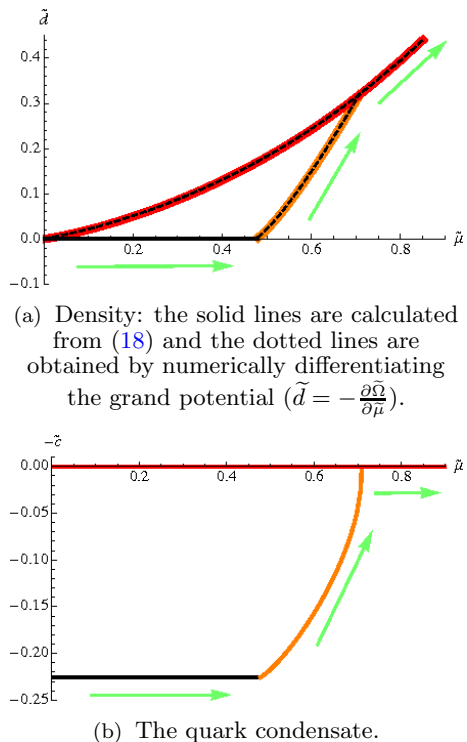


FIG. 4: Plots of the order parameters vs chemical potential at zero temperature and finite  $B$ . Both are continuous across the Minkowski to spiky embedding transition ( $\tilde{\mu} \sim 0.47$ ). The green arrows indicate the changes of phase.

order (or so weakly first order that it can be treated as second order). This second order nature of the transition from a Minkowski to a spiky embedding has been shown also in the  $B = 0, \tilde{m} \neq 0$  case at zero temperature analytically [15] and numerically [16].

Finally, above the chemical potential corresponding to the meson melting transition ( $\tilde{\mu} = 0.470$ ), non-zero density is present and the physics already described in the Canonical Ensemble occurs, which turns out to be equivalent to the results from the current Grand Canonical Ensemble. Both Ensemble predict the second order transition to the flat embedding at the same point,  $\tilde{\mu} = 0.708$  or  $\tilde{d} = 0.3197$ , which is the chiral symmetry restoration point. Notice that for the Canonical Ensemble we used  $(\tilde{m}, \tilde{c})$  conjugate variables on constant  $\tilde{d}$  slices, while for the Grand Canonical Ensemble we used  $(\tilde{\mu}, \tilde{d})$  conjugate variables on constant  $\tilde{m} = 0$  slices. This agreement from different approaches is another consistency check of our calculation.

On the gauge theory side of the dual, the description is as follows. At zero density there is a theory with chiral symmetry breaking and bound mesons. As the chemical potential is increased  $\tilde{d}$  remains zero and the quark condensate remains unchanged. Then there is a second order transition to finite density (to a spike like embedding) which is presumably associated with meson melting induced by the medium. At a higher density there

is then a further second order transition to a phase with zero quark condensate.

Finally we note a recent paper [34] that proposed an alternative ground state for a chiral symmetry breaking theory at finite density. They proposed that the string spike might end on a wrapped D5 brane baryon vertex in the centre of the geometry. We have not considered that possibility here but it might be interesting to investigate this in the future. The magnetic field induced chiral symmetry breaking provides a system in which this could be cleanly computed without the worries of the hard wall present in that geometry.

## V. THE PHASE DIAGRAM IN THE GRAND CANONICAL ENSEMBLE

We have identified a first order phase transition from a chiral symmetry breaking phase with meson bound states to a chirally symmetric phase with melted mesons in our massless theory in the presence of a magnetic field with increasing pure temperature. On the finite density axis the meson melting transition is second order and separate from another second order chiral symmetry restoring phase transition. Clearly there must be at least one critical point in the temperature chemical potential phase diagram. We display the phase diagram of the massless theory, which we will discuss the computation of, in Fig 5.

To construct the phase diagram we have plotted slices at fixed temperature and varying chemical potential. We display the results in Fig 3a-e where we show the embeddings (Left) relevant at different temperatures, their trajectories in the  $\tilde{d} - \tilde{\mu}$  plane (Middle) and the grand potential (Right).

The phase diagram agrees with our previous results: At zero chemical potential we have the transition point  $\tilde{w}_H = 0.2516$ . At zero temperature we have the transition point at  $\tilde{\mu} = 0.708$ , which corresponds to  $\tilde{d} = 0.3197$ . We also identify  $\tilde{\mu} = 0.470$  as the position of the second order

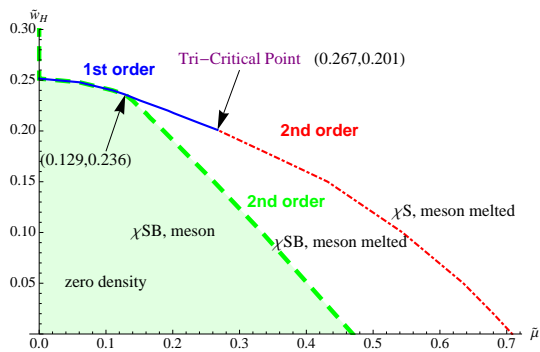


FIG. 5: The phase diagram of the  $\mathcal{N} = 2$  gauge theory with a magnetic field. The temperature is controlled by the parameter  $\tilde{w}_H$  and chemical potential by  $\tilde{\mu}$ . (Parameters are scaled or  $B = 1/2R^2$  in terms of parameters without tilde.)

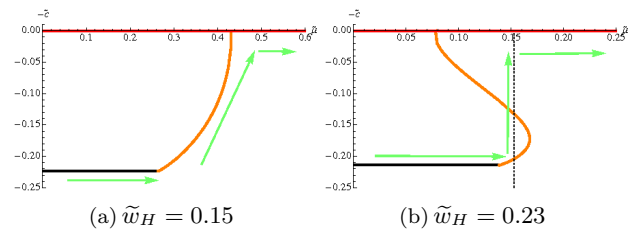


FIG. 6: Quark condensate vs chemical potential at finite  $B$ . Both are continuous across the Minkowski (black) to black hole (orange) embedding transition. At  $\tilde{w}_H = 0.23$  the black hole (orange) to black hole (red) transition is discontinuous.

transition to a meson melted phase with non-zero  $\tilde{d}$  and chiral condensate  $\tilde{c}$ .

The dotted green line is the line along which  $\tilde{d} = 0$  and corresponds to the second order meson melting transition from a Minkowski embedding to a black hole embedding. The transition generates density continuously from zero. The quark condensate also smoothly decreases from its constant value on the Minkowski embedding. We display the continuous behaviour of the quark condensate across the transition in Fig 6. Note this means that the slope of the embedding at the UV boundary is continuous through the transition even though the embedding in the IR is discontinuous and topology changing. Again we have checked the smoothness of these parameters numerically to better than the 1% level.

The blue line corresponds to a first order transition in density, chiral condensate etc. The red dotted line is rather special in that this is a phase boundary only at  $\tilde{m} = 0$ . This is because this phase boundary is related to the spontaneous breaking of chiral symmetry which only exists at  $\tilde{m} = 0$ . At finite  $\tilde{m}$  it must be a cross over region as we will discuss further in section VII

The diagram then displays two tri-critical points. It is straightforward to identify where the points lie numerically. The chiral symmetry tri-critical point where the

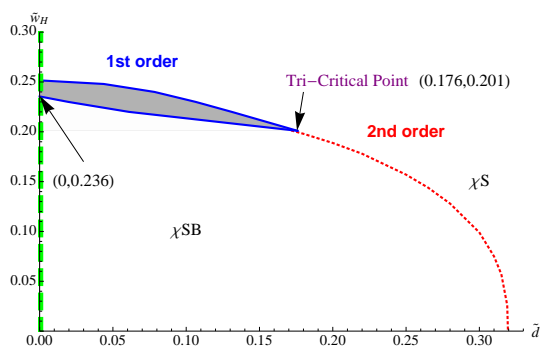


FIG. 7: The phase diagram of the  $\mathcal{N} = 2$  gauge theory with a magnetic field. The temperature is controlled by the parameter  $\tilde{w}_H$  and the density by  $\tilde{d}$ . (Parameters are scaled or  $B = 1/2R^2$  in terms of parameters without tilde.)

first and second order chiral symmetry restoration transitions join lies at the point  $(\tilde{\mu}, \tilde{w}_H) = (0.267, 0.201)$ . The second tri-critical point where the meson melting transitions join is at  $(\tilde{\mu}, \tilde{w}_H) = (0.129, 0.236)$ .

## VI. THE PHASE DIAGRAM IN THE CANONICAL ENSEMBLE

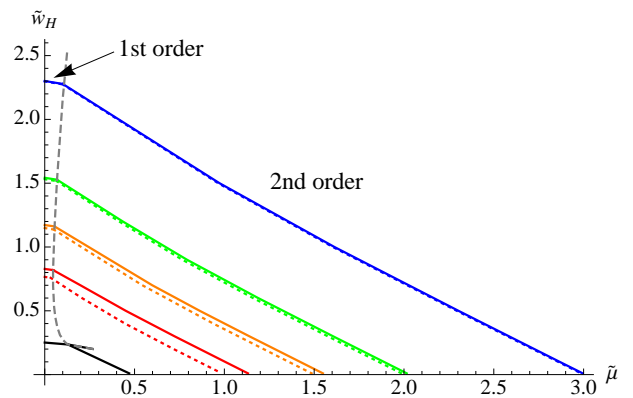
We can study the phase diagram also in the canonical ensemble. It is shown in Fig 7 and has the same information as Fig 5. The pale green region in Fig 5 lies in the green dotted line along the  $\tilde{w}_H$  axis of Fig 7. The chiral symmetry breaking region enclosed by the red, green and blue lines in each figure map onto each other. Similarly the high temperature and density region to the upper right of all the lines in both plots map onto each other. The two double blue lines and the area between them in Fig 7 correspond to the single blue line in Fig 5, which is natural since the blue line in Fig 5 is a first order transition line and the density change is discontinuous. Thus the gray region in Fig 7 is an unstable density region which hides in the phase boundary in Fig 5. That region may only be reached by super-cooling or super-heating since it is unstable. The true ground state at those densities and temperatures should be a mixture of the black hole and Minkowski embedding in analogy with the liquid-gas mixture between the phase transition's of water [16]. It's not clear how to realize that mixture in a holographic set-up.

## VII. FINITE MASS

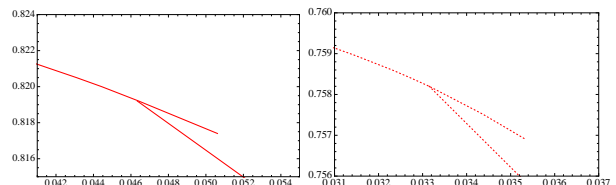
We next describe the evolution of the phase diagram with quark mass. If we move away from zero quark mass then the second order chiral symmetry restoration phase transition at  $T=0$  but growing chemical potential becomes a cross over transition. This can be seen in Fig 2 where for  $\tilde{m} \neq 0$  the non-zero value of the condensate can be seen to change smoothly with changing  $\tilde{\mu}$  and there is no jump in any order parameter. The (chiral) tri-critical point becomes a critical point. However, the other transition lines survive the introduction of a quark mass.

In Fig 8. we plot the phase diagram for various quark mass,  $\tilde{m}$ , at constant  $B$ . The colors represent different quark masses -  $\tilde{m} = 0, 1, 1.5, 2, 3$  from bottom to top are black, red, orange, green, and blue. The solid lines are for finite, fixed  $B$ . To show the influence of the magnetic field we also display the  $B = 0$  solution as the dotted lines. The gray line shows the motion of the critical points.

In general the magnetic field shifts the transition line up and right, meaning that the magnetic field makes the meson more stable against the temperature/density meson dissociation effect. This is important at small  $\tilde{m}$  but negligible at large  $\tilde{m}$  as expected.



(a) The curves correspond to  $\tilde{m} = 0$ (black), 1(red), 1.5(orange), 2(green), 3(blue) from bottom to top. The gray line is the path of the critical points.



(b) A zoom into figure (a) to show the critical point structure at small chemical potential. Here we show the detail of  $\tilde{m} = 1$  case, but a similar structure exists for every case.

FIG. 8: The phase diagram at finite current quark mass with finite  $B$  (solid lines) and zero  $B$  (dotted lines).

Both critical points survive the introduction of a finite  $\tilde{m}$ , even though it looks like there is no critical point in Fig 8a. Zooming in on the appropriate region at small chemical potential reveals the two critical point structure as shown in Fig 8b. Their positions, as  $\tilde{m}$  changes, are marked by the gray line in Fig 8a. The one line represents the two critical points which are indistinguishable close on the scale of Fig 8a. The chiral symmetry critical point moves very close to the other critical point even for a very small mass ( $\tilde{m} \sim 0.01$ ). The interpretation of the critical points and the phase boundaries are the same as in the  $\tilde{m} = 0$  case in the previous section.

Notice that the black hole to black hole transition exists even in the  $B=0$  case as shown in Fig 8b(Right), so it is not purely due to the magnetic field. Nevertheless this transition seems not to have been reported in the previous works [14, 16]. We believe that this is because the transition line between the two critical points is too small to be resolved on the scale of Fig 8a, which agrees qualitatively with the figures in [16]. In order to find those transitions we had to slice the temperature down to order  $10^{-3}$  as shown on the vertical axis in Fig 8b(Right). Any coarser graining would miss it.

The final surprise relative to the previous work is that the meson melting transition below the critical point appears second order in our work even in the infinite mass limit. To emphasize this we show a number of plots in

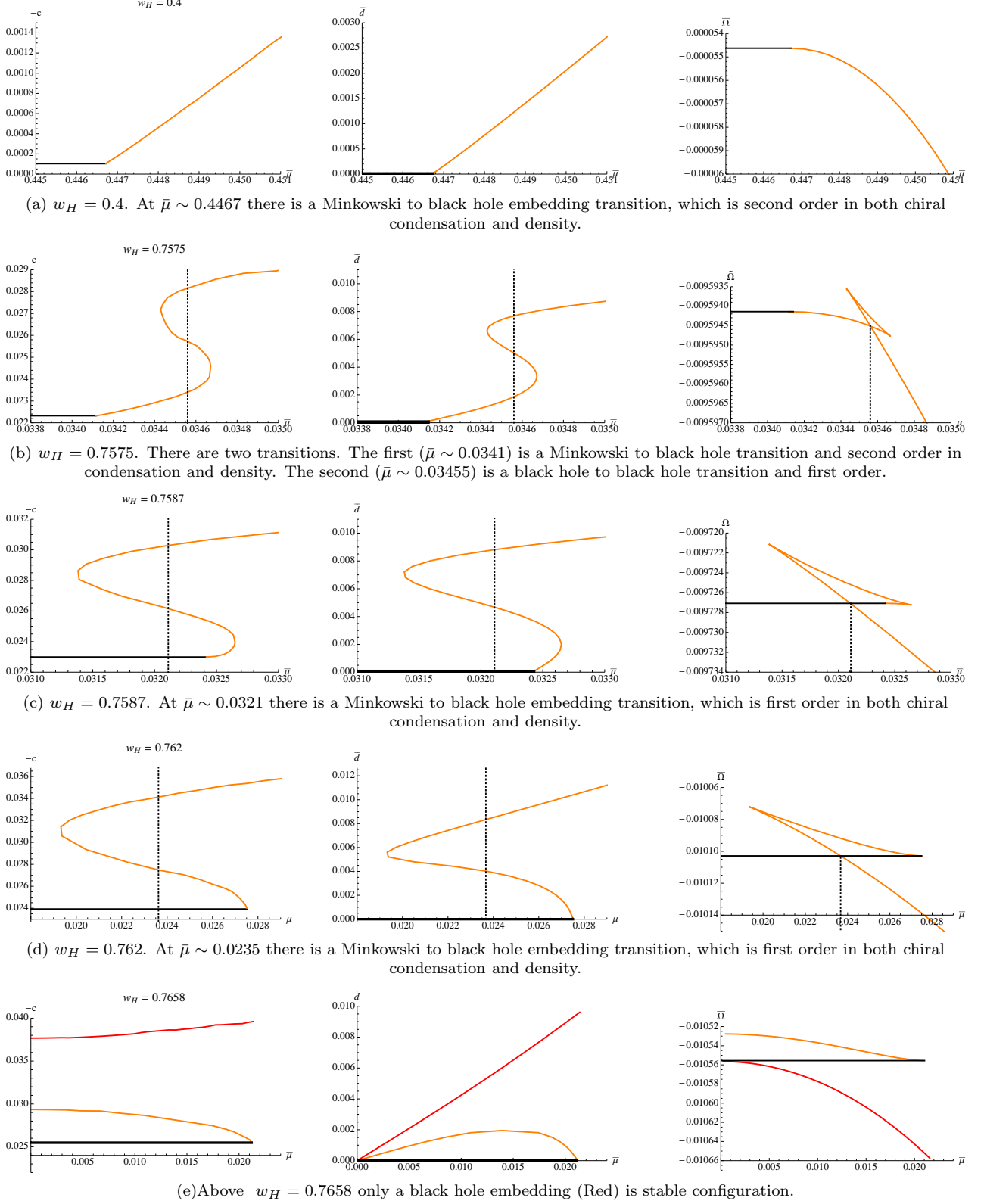


FIG. 9: Chiral condensation (Left), density (Middle), and the grand potentials (Right) for massive quarks ( $m = 1$ ) at  $B = 0$  at a variety of temperatures that represent slices through the phase diagram Fig 8a.

the  $B = 0$  theory in Fig 9.

Since the scaled variables (16) cannot be used at  $B = 0$ , (20) and (18) read in terms of the original coordinates:

$$\begin{aligned} \bar{\Omega}(w_H, \bar{\mu}) &:= \frac{-S}{N_f T_{D7} \text{Vol}} \\ &= \int_{\rho_H}^{\infty} d\rho \frac{w^4 - w_H^4}{w^4} \sqrt{\frac{(1 + (L')^2)}{K}} \left( \frac{w^4 + w_H^4}{w^4} \right)^2 \rho^6, \end{aligned} \quad (21)$$

where

$$\bar{\mu} = \int_{\rho_H}^{\infty} d\rho \bar{d} \frac{w^4 - w_H^4}{w^4 + w_H^4} \sqrt{\frac{1 + (L')^2}{K}}, \quad (22)$$

$$K = \left( \frac{w^4 + w_H^4}{w^4} \right)^2 \rho^6 + \frac{w^4}{(w^4 + w_H^4)} \bar{d}^2, \quad (23)$$

$$\bar{\mu} := \sqrt{2}^3 \pi \alpha' A_t(\infty), \quad \bar{d} := \frac{\sqrt{2}^3}{N_f T_{D7} 2\pi \alpha'} d \quad (24)$$

By the same procedures as in the previous sections we get Fig 9. Compared to Fig 3, the left column of Fig 9 is the chiral condensate instead of the embedding configurations. In Fig 3 there is always a red black hole embedding, which corresponds to the flat embedding at zero quark mass. It is not present at finite quark mass.

At very low temperature the transition is Minkowski to black hole and *second order* in the condensate and density (Fig 9a). As the temperature goes up a *new* black hole to black hole transition pops up by developing a ‘swallow tail’ in the grand potential - this transition is first order in the condensate and density (Fig 9b). As temperature rises the ‘swallow tail’ grows continually and eventually “swallows” the *second order* Minkowski to black hole transition (Fig 9 c,d). *i.e.* At higher temperature the *second order* Minkowski to black hole transition enters an unstable regime and plays no role any more. Instead only the *first order* Minkowski to black hole transition is manifest. Finally the Minkowski embedding becomes unstable compared to the black hole embedding (Fig 9e). At an even higher temperature the Minkowski embedding is not allowed and only a black hole embedding is available (Not shown in Fig 9).

These results all match with our work at finite  $B$  and increasing mass, confirming those results and our phase diagrams already presented.

### VIII. COMPARISON TO QCD

We have computed the phase diagram for a particular gauge theory using holographic techniques. There are many differences between our theory and QCD: the theory has super partners of the quarks and glue present; it is at large  $N$  and small  $N_f$ , so quenched (and we have only computed for degenerate quarks to avoid complications involving the non-abelian DBI action); the theory

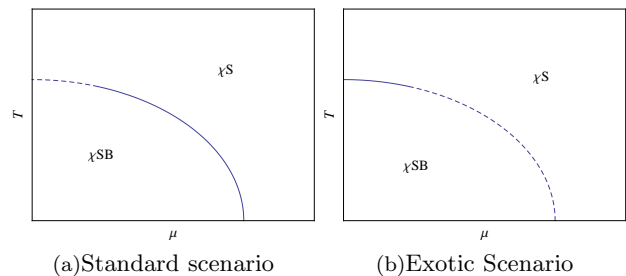


FIG. 10: Two possible phase diagrams for QCD with the observed quark masses. (a) is the standard scenario found in most of the literature but a diagram as different as (b) remains potentially possible according to the work in [3]. We have not included any color superconducting phase here at large chemical potential.

has deconfined glue for all non-zero temperature; the theory has a distinct meson melting transition. In spite of these differences the phase diagram for the chiral condensate shows many of the aspects of the QCD phase diagram so we will briefly make a comparison here.

The QCD phase diagram is in fact not perfectly mapped out since there have only recently been lattice computations attempting to address finite density [3]. The phase structure also depends on the relative masses of the up, down and strange quarks. The standard theoretical picture [1–3] for physical QCD is shown in Fig 10a. At zero chemical potential the transition with temperature is second order (or a cross over with massive quarks). At zero temperature there is a first order transition with increasing chemical potential (ignoring any superconducting phase). These transitions are joined by a critical point. Comparing to our theory in Fig 5 we see that the transitions’ orders are reversed and the pictures look rather different.

In fact though as argued in [3] the picture could be very different in QCD. At zero quark mass the finite temperature transition is first order and whether it has changed to second order depends crucially on the precise physical quark masses. Similarly whether the finite density transition is truly first order or second order depends on the exact physical point in the  $m_{u,d}, m_s, \mu, T$  volume. Arguments can even be made for a phase diagram matching that in Fig 10b which then matches the structure of the chiral symmetry restoring phase diagram of the theory we have studied. For the true answer in QCD we must wait on lattice developments. Clearly our model will not match QCD’s phase diagram point by point in  $m_{u,d}, m_s, \mu, T$  volume but it provides an environment in which clear computation is possible for structures that match some points in that phase space.

Finally, we note a more general point that seems to emerge from the analysis. The introduction of a chemical potential weakens the first order nature of the transitions in our analysis. This matches with results found in QCD on the lattice. The weakening of the first order phase transition is demonstrated for the chiral transition

in the light quark mass regime [35, 36], and is shown for the deconfinement transition in the heavy quark mass regime [37, 38].

**Acknowledgements:** NE and KK are grateful for the support of an STFC rolling grant. KK would like

to thank Owe Philipsen, Sang-Jin Sin, Yunseok Seo, Johanna Erdmenger, and Ingo Kirsch for discussions. AG and MM are grateful for University of Southampton Mayflower Scholarships.

- 
- [1] K. Rajagopal and F. Wilczek, arXiv:hep-ph/0011333.  
 [2] M. A. Stephanov, PoS **LAT2006** (2006) 024 [arXiv:hep-lat/0701002].  
 [3] O. Philipsen, arXiv:0910.0785 [hep-ph].  
 [4] J. M. Maldacena, Adv. Theor. Math. Phys. **2**, 231 (1998) Int. J. Theor. Phys. **38**, 1113 (1999) [arXiv:hep-th/9711200].  
 [5] E. Witten, Adv. Theor. Math. Phys. **2** (1998) 253 [arXiv:hep-th/9802150].  
 [6] S. S. Gubser, I. R. Klebanov and A. M. Polyakov, Phys. Lett. B **428** (1998) 105 [arXiv:hep-th/9802109].  
 [7] A. Karch and E. Katz, JHEP **0206**, 043 (2002) [arXiv:hep-th/0205236].  
 [8] M. Grana and J. Polchinski, Phys. Rev. **D65** (2002) 126005, [arXiv: hep-th/0106014].  
 [9] M. Bertolini, P. Di Vecchia, M. Frau, A. Lerda and R. Marotta, Nucl. Phys. B **621**, 157 (2002) [arXiv:hep-th/0107057].  
 [10] M. Kruczenski, D. Mateos, R. C. Myers and D. J. Winters, JHEP **0307** 049, 2003 [arXiv:hep-th/0304032].  
 [11] J. Erdmenger, N. Evans, I. Kirsch and E. Threlfall, Eur. Phys. J. A **35** (2008) 81 [arXiv:0711.4467 [hep-th]].  
 [12] S. Nakamura, Y. Seo, S. J. Sin and K. P. Yogendran, J. Korean Phys. Soc. **52**, 1734 (2008) [arXiv:hep-th/0611021].  
 [13] S. Kobayashi, D. Mateos, S. Matsuura, R. C. Myers and R. M. Thomson, JHEP **0702**, 016 (2007) [arXiv:hep-th/0611099].  
 [14] S. Nakamura, Y. Seo, S. J. Sin and K. P. Yogendran, Prog. Theor. Phys. **120**, 51 (2008) [arXiv:0708.2818 [hep-th]].  
 [15] A. Karch and A. O'Bannon, JHEP **0711**, 074 (2007) [arXiv:0709.0570 [hep-th]].  
 [16] D. Mateos, S. Matsuura, R. C. Myers and R. M. Thomson, JHEP **0711** (2007) 085 [arXiv:0709.1225 [hep-th]].  
 [17] K. Ghoroku, M. Ishihara and A. Nakamura, Phys. Rev. D **76**, 124006 (2007) [arXiv:0708.3706 [hep-th]].  
 [18] K. Peeters, J. Sonnenschein and M. Zamaklar, Phys. Rev. D **74** (2006) 106008 [arXiv:hep-th/0606195].  
 [19] C. Hoyos-Badajoz, K. Landsteiner and S. Montero, JHEP **0704** (2007) 031 [arXiv:hep-th/0612169].  
 [20] J. Erdmenger, M. Kaminski and F. Rust, Phys. Rev. D **77**, 046005 (2008) [arXiv:0710.0334 [hep-th]]; J. Erdmenger, C. Greubel, M. Kaminski, P. Kerner, K. Landsteiner and F. Pena-Benitez, arXiv:0911.3544 [hep-th].  
 [21] V. G. Filev, C. V. Johnson, R. C. Rashkov and K. S. Viswanathan, JHEP **0710**, 019 (2007) [arXiv:hep-th/0701001]; V. G. Filev, JHEP **0804**, 088 (2008) [arXiv:0706.3811 [hep-th]]; T. Albash, V. G. Filev, C. V. Johnson and A. Kundu, JHEP **0807**, 080 (2008) [arXiv:0709.1547 [hep-th]].  
 [22] J. Erdmenger, R. Meyer and J. P. Shock, JHEP **0712**, 091 (2007) [arXiv:0709.1551 [hep-th]].  
 [23] A. V. Zayakin, and Goldstone Mass," JHEP **0807** (2008) 116 [arXiv:0807.2917 [hep-th]].  
 [24] V. G. Filev, C. V. Johnson and J. P. Shock, JHEP **0908**, 013 (2009) [arXiv:0903.5345 [hep-th]]; V. G. Filev, JHEP **0911**, 123 (2009) [arXiv:0910.0554 [Unknown]].  
 [25] S. S. Gubser, arXiv:hep-th/9902155.  
 [26] L. Girardello, M. Petrini, M. Porrati and A. Zaffaroni, Nucl. Phys. B **569** (2000) 451 [arXiv:hep-th/9909047].  
 [27] K. Y. Kim, S. J. Sin and I. Zahed, arXiv:hep-th/0608046; K. Y. Kim, S. J. Sin and I. Zahed, JHEP **0801**, 002 (2008) [arXiv:0708.1469 [hep-th]].  
 [28] J. Babington, J. Erdmenger, N. J. Evans, Z. Guralnik and I. Kirsch, Phys. Rev. D **69** (2004) 066007 [arXiv:hep-th/0306018].  
 [29] R. Apreda, J. Erdmenger, N. Evans and Z. Guralnik, Phys. Rev. D **71** (2005) 126002 [arXiv:hep-th/0504151].  
 [30] T. Albash, V. G. Filev, C. V. Johnson and A. Kundu, Phys. Rev. D **77** (2008) 066004 [arXiv:hep-th/0605088].  
 [31] D. Mateos, R. C. Myers and R. M. Thomson, Phys. Rev. Lett. **97** (2006) 091601 [arXiv:hep-th/0605046].  
 [32] D. Mateos, R. C. Myers and R. M. Thomson, JHEP **0705**, 067 (2007) [arXiv:hep-th/0701132].  
 [33] S. Nakamura, Prog. Theor. Phys. **119**, 839 (2008) [arXiv:0711.1601 [hep-th]].  
 [34] Y. Seo, J. P. Shock, S. J. Sin and D. Zoakos, arXiv:0912.4013 [hep-th].  
 [35] P. de Forcrand and O. Philipsen, JHEP **0811** (2008) 012 [arXiv:0808.1096 [hep-lat]].  
 [36] P. de Forcrand and O. Philipsen, JHEP **0701** (2007) 077 [arXiv:hep-lat/0607017].  
 [37] J. Langelage and O. Philipsen, arXiv:0911.2577 [hep-lat].  
 [38] S. Kim, Ph. de Forcrand, S. Kratochvila and T. Takaishi, PoS **LAT2005** (2006) 166 [arXiv:hep-lat/0510069].